Solar Energy Materials & Solar Cells 158 (2016) 160–167

Contents lists available at ScienceDirect

Solar Energy Materials & Solar Cells

journal homepage: www.elsevier.com/locate/solmat

Energy structure of CdSe/CdTe type II colloidal quantum dots—Do phonon bottlenecks remain for thick shells?

Charles T. Smith [a], Edward J. Tyrrell [b], Marina A. Leontiadou [a], Jacek Miloszewski [b], Thomas Walsh [b], Musa Cadirci [a], Robert Page [c], Paul O'Brien [c], David Binks [a], Stanko Tomić [b,*]

[a] School of Physics and Astronomy & Photon Science Institute, University of Manchester, Manchester M13 9PL, United Kingdom
[b] Joule Physics Laboratory, School of Computing, Science and Engineering, University of Salford, Manchester M5 4WT, United Kingdom [c]School of Chemistry, University of Manchester, Manchester M13 9PL, United Kingdom
[c] School of Chemistry, University of Manchester, Manchester M13 9PL, United Kingdom

ARTICLE INFO

Article history:
Received 23 July 2015
Received in revised form
20 November 2015
Accepted 13 December 2015
Available online 13 January 2016

Keywords:
Efficiency
Absorption
Solar cells
Colloidal quantum dots
Core/shell structure

ABSTRACT

The electronic structures of CdSe/CdTe type II colloidal quantum dots are predicted using a model based on $\mathbf{k}\cdot\mathbf{p}$ theory and the many-particle configuration interaction method. The separation of energy levels in the conduction band is examined and used to identify phonon bottlenecks, and how these evolve as the shell thickness is increased. Bottlenecks are found to persist both above and below the threshold for multiple exciton generation for all the shell thicknesses investigated. The overall electron cooling rate is thus expected to fall as the shell thickness is increased and Auger cooling suppressed, and this is confirmed experimentally using ultrafast transient absorption measurements. A reduced overall rate of electron cooling will enhance the quantum yield of multiple exciton generation with which it competes. Using a detailed-balance model, we have thus calculated that with proper design of core/and shell structures the efficiency of a solar cell based on CdSe/CdTe quantum dots can be enhanced to 36.5% by multiple exciton generation.

1. Introduction

In bulk semiconductors, the energy of an absorbed photon in excess of the band gap E_g is lost by phonon emission in about a picosecond as the initially hot carriers cool to the band edge through a continuum of states. This carrier thermalization is an important energy loss mechanism in solar cells, corresponding to almost 50% of the incident solar energy for silicon photovoltaic devices under unconcentrated sunlight [1]. However, for colloidal quantum dots (CQDs) i.e. semiconductor nano-crystals produced by solvent-based synthesis routes, confinement of the carrier wave-function by the nano-scale dimensions of the crystal causes both the conduction band (CB) and valence band (VB) to change into a set of discrete electronic states. The energy separation of these states increases as the size of the CQD is reduced and for sufficiently small sizes will exceed the phonon energy, particularly in the CB where the typically smaller effective mass of the electron compared to that of the hole, results in greater energy level separation. For example, the separation of states in the CB of CdSe CQDs can be larger than 300 meV, an order of magnitude greater than the phonon energy of ~30 meV in this material [2]. Such a large energy level separation relative to the phonon energy will significantly reduce the rate of electron cooling by phonon emission, which now must involve multiple rather than single phonons and is consequently much less probable. Indeed, the recognition that the rate of phonon emission will be significantly decreased for small CQDs (which became known as the "phonon bottleneck") led to the expectation that the carrier cooling lifetime would be greatly increased in CQDs [3]. Extending the time before carrier thermalization is an important goal because it could enable the solar energy lost to heat to be usefully harvested instead. This could be accomplished by extracting the carriers before they cool in a "hot-carrier solar cell" which would enhance the photo-voltage, or by using the energy of the hot carriers to generate additional electron-hole pairs by multiple exciton generation (MEG), also known as carrier multiplication, and thus increase the photocurrent [4–6]. However, the electron cooling lifetime in CQDs was found experimentally to be typically a few picoseconds [7–11] despite the large energy separations in the CB, indicating that

* Corresponding author. Tel.: +44 0 161 295 3847.
E-mail address: s.tomic@salford.ac.uk (S. Tomić).

http://dx.doi.org/10.1016/j.solmat.2015.12.015

cooling processes other than phonon emission are important in CQDs. These processes include Auger relaxation whereby a hot electron cools to the band edge by transferring energy to a hole, which has already cooled by phonon emission due to the typically much smaller energy level separation in the VB [2,12–14]. Trap states formed by the under coordination of atoms on the CQD surface provide additional pathways for carrier relaxation, increasing the overall rate of cooling [15]. Recently, effective passivation of surface traps with chloride ions was found to reduce the rate of cooling by 46% in CdTe CQDs [11]. Finally, energy transfer to the organic ligands (used to passivate the CQD surface and prevent agglomeration) is another relaxation pathway [16] that can lead to a reduced cooling lifetime. These various cooling processes compete with hot carrier extraction and MEG, reducing their quantum yield and thus the potential benefit they bring to solar cell performance. For instance, if MEG were the dominant mechanism by which hot electrons eventually reach the band edge, the efficiency of an ideal solar cell would increase from the Shockley–Queisser limit of 33% (which assumes hot carrier thermalisation) to 44% [17]. However, only modest improvements in quantum yield have been reported, which if exploited in a solar cell would not lead to a significant improvement in efficiency [18]; this under-performance has been attributed to the effect of the competition between MEG and the cooling processes described above [4,19]. Nevertheless, the synthesis techniques developed over the years for CQDs afford means by which their structure and composition can be modified to suppress the unwanted cooling processes that compete with MEG and hot carrier extraction, and thereby improve solar cell performance. A shell of a different semiconductor material can be grown around a CQD to produce what is known as a type II structure; this forms a heterojunction, the band alignment of which causes CB electrons to localise in one region and holes to localise in the other [20,21]. This localisation reduces the wave-function overlap of the two carriers and thus reduces the rate of Auger relaxation. A greater understanding of how unsaturated surface atoms form trap states and how different ligands interact with the CQD surface has enabled effective passivation strategies to be developed [22]. For instance, unsaturated surface Cd atoms are known to produce electron traps but these can be effectively passivated by a ligand with an amine group [22,23]. A combination of these approaches enabled Pandey et al. to demonstrate in type II CdSe/ZnSe CQDs an electron cooling lifetime between the lowest two CB states that was $\sim$1 ns [2]. Controlling the cooling rate between states lying higher in the CB is key to the reduction of thermalisation losses since it is these states that are most important to both MEG and hot carrier cells. The threshold for MEG corresponds to the photon energy that produces hot electrons that have an energy above the CB minimum that is equal to E_g, i.e. the minimum needed to promote an additional electron across the band gap. Furthermore, since the peak solar irradiance corresponds to photons with an energy of $\sim$2.5 eV, for solar cells with the optimal absorption edge at about 1.3 eV [24], many of the CB electrons created by the absorption of a solar photon will be in higher lying states. An efficient hot carrier cell must thus extract electrons from these higher lying states before cooling. Using a type II CQD structure to reduce cooling from these high energy states involves a trade-off between different processes: whilst increasing the shell thickness will reduce Auger cooling, it will also reduce the separation between levels. If this energy separation is reduced so that it is similar to the phonon energy then phonon cooling will become significantly greater, potentially negating any reduction in overall cooling achieved by reducing Auger relaxation.

In this work, detailed modelling of the energy level structure of type II CdSe/CdTe CQDs is presented, and the shift in the energy levels produced by increasing shell thickness for different core sizes is reported. In particular, the separation between levels in the CB is examined to an energy of greater than E_g above the band edge. This allows the confirmation for the first time that the addition of a shell intended to reduce the Auger cooling that competes with MEG, does not at the same time remove the energy level bottleneck that prevents phonon cooling competing with MEG. The cooling behaviour expected from this analysis is compared to example experimental data for type II CdSe/CdTe CQDs, with good agreement found between the model and observation. Using a detailed balance model, we have calculated the efficiency of solar cells based on CdSe/CdTe type II core/shell CQDs with and without MEG for several characteristic core dimensions and over a range of shell thicknesses. The corresponding variation in short circuit current, J_{sc} and open circuit voltage, V_{oc}, under idealised conditions is also detailed.

2. Methodology

2.1. Theory

In order to describe the electronic structure of CdSe/CdTe CQDs we perform calculations using $\mathbf{k}\cdot\mathbf{p}$ theory in conjunction with the configuration interaction (CI) method. The 8-band $\mathbf{k}\cdot\mathbf{p}$ Hamiltonian $\hat{H}$ for spherically symmetric CQD heterostructures [25] is used to calculate single-particle states; this theory takes into account CB-VB coupling [26], the complex VB structure, the spin-orbit interaction and correct operator ordering at the core/shell heterointerface. The Schrödinger equation for the single-particle states can be written as

$$\hat{H}\psi_{n,j,m,p} = E_{n,j,p}\psi_{n,j,m,p} \tag{1}$$

where $\psi_{n,j,m,p}$ is the single-particle wave function, $E_{n,j,p}$ is the single-particle energy, n is the principle quantum number, j is the total angular momentum, m is the z-component of the total angular momentum and p is the eigenvalue of the parity operator. In the 8-band $\mathbf{k}\cdot\mathbf{p}$ theory the single-particle wave function is given by [25]:

$$\psi_{njmp}(\mathbf{r}) = \sum_{b=1}^{8}\sum_{J(b)}\sum_{J_z(b)} F_{J,J_z}^{b;njmp}(\mathbf{r})u_{J,J_z}^{b} \tag{2}$$

where index $b=1,\ldots,8$, corresponds to each of 8 spin degenerate bands, u_{J,J_z}^{b} represents the Bloch functions of each band, $J(b)$ and $J_z(b)$ are the Bloch function angular momentum and is its z-component of each band, $F_{J,J_z}^{b;njmp}(\mathbf{r})$ are envelope functions which contain the angular and radial dependencies of the wave functions; full definitions are given in [25,26]. Due to the spherical symmetry of the system, eigenenergies are $(2j+1)$-fold degenerate with respect to the quantum number m. The eigenenergies of single-particle levels are calculated by numerically solving the equations resulting from imposing continuity of the radial wave functions and radial component of the probability current across the heterointerfaces [25]. We denote single-particle states using the spectroscopic notation $nl_j^{(\mu)}$ where $l=s,p,d,\ldots$ represents the lowest value of the orbital angular momentum in the wave function. The eigenvalue p of the parity operator takes the values 1 and -1 for even and odd symmetry states respectively.

In contrast to epitaxial QDs [27], the large dielectric mismatch between CQDs and the surrounding solvent necessitates the inclusion of self-polarization terms in the Hamiltonian. Such dielectric confinement has been shown to have a significant effect on the correlated exciton wave functions and energies in CdSe/CdTe CQDs [21], so its effect on the excitonic structure should not be neglected. In the presence of a spatially-varying dielectric

constant the exciton Hamiltonian may be written as:

$$\hat{H}_X = \hat{H} + V_c(\mathbf{r}_e, \mathbf{r}_h) + V_s(\mathbf{r}_e) + V_s(\mathbf{r}_h) \quad (3)$$

where V_c is the interparticle Coulomb potential and V_s is the self-polarization potential due to the interaction of a carrier with its own polarization charge. We note that $V_c = V_p + V_d$ where V_d is the direct interparticle Coulomb potential and V_p is the interface polarization potential [28]. We calculate the potentials V_c and V_s using the numerical model of Bolcatto and Proetto for finite size dielectric interfaces [29].

Correlated exciton states are solutions of the Schrödinger equation

$$\hat{H}_X \Psi_X^{L,L_z} = E_X \Psi_X^{L,L_z} \quad (4)$$

where L is the total exciton angular momentum, L_z is its z-component and E_X is the exciton eigen-energy. To construct excitonic states, we couple single-particle states in terms of angular momentum rather than parity [25]. We expand the exciton wave function in terms of uncorrelated electron-hole pair (EHP) states, obtained from Eq. (1), as [30]:

$$\Psi_X^{L,L_z} = \sum_\beta c_\beta |\, n_e l_e j_e n_h l_h j_h; L, L_z\rangle \quad (5)$$

where

$$|\, n_e l_e j_e n_h l_h j_h; L, L_z\rangle = \sum_{m_e, m_h} C^{L,L_z}_{j_e m_e j_h m_h} |\, n_e l_e j_e m_e\rangle |\, n_h l_h j_h m_h\rangle \quad (6)$$

and $C^{L,L_z}_{j_e m_e j_h m_h}$ and c_β represent a Clebsch–Gordan coefficient and the expansion coefficient (character) of a particular EHP state labeled by β, respectively. The exciton Hamiltonian is then diagonalized in the basis of EHPs to find the exciton energies and wave functions; this is sometimes called direct diagonalization or the configuration interaction (CI) method [27].

2.2. CQD synthesis

CdSe cores with a zinc-blende crystal structure were grown using a hot-injection technique and dual precursors, as previously reported in Ref. [31]. The CdTe shell was added by a dropwise method, as described in Ref. [32]. After the shelling process was completed, the CQDs were cooled at room temperature and stored in a nitrogen atmosphere.

2.3. Transient absorption spectrometer

The sub-nanosecond exciton dynamics were studied using an ultrafast transient absorption spectrometer. In this pump-probe technique we use the output beam of a mode-locked Ti:Sapphire oscillator–amplifier laser system (Spectra Physics, SpitfirePro) to produce 100 fs, 1 mJ pulses at a repetition rate of 1 kHz. A beam splitter directs 95% of the amplifier output to an optical parametric amplifier (Light Conversion, TOPAS) with subsequent harmonic generation which produces a pump beam tunable in the ultraviolet and visible parts of the spectrum. The remaining part of the laser system output was directed through a 2 mm thick sapphire crystal in order to create a white light continuum which acts as the probe beam. The probe beam was focussed to a 1 mm spot size at the sample position and tuned at the first absorption peak photon energy. The pump beam was modulated at 500 Hz with the use of an optical chopper and bypassed the sample with a photon energy of 2.76 eV and a fluence of 50 μJ/cm^2. The probe beam was directed into a monochromator (SpectroPro 2500i) and the changes in the sample absorbance induced by the pump beam were detected by two silicon photodiodes. The samples under investigation were diluted, placed in 10 mm thick quartz cuvettes and stirred by a magnetic stirrer (Thermo Scientific, Variomag Mini) at 1000 rpm throughout the experiments. More details on the experimental technique can be found in [7,8,11] and references therein.

3. Results and discussions

3.1. Excitonic structure

In materials with polar bonds like CdSe, or CdSe/CdTe QDs, the optical phonons couple to electronic excitations. We begin our analysis with detailed examination of the excitonic structure obtained using the CI method as described in Section 2.1. In Table 1, we show the difference between the first few lowest excitonic states of an a_c=2 nm CdSe core-only CQD (a_s=0 case) and a set of CdSe/CdTe core/shell CQDs with shell thicknesses varying from a_s=0.5 to 3.0 nm. By changing the shell thickness from a_s=0 (no shell) to a_s=3 nm the excitonic ground state energy, E_{X0}, is changed from 2.30 eV to 1.49 eV. It is interesting to note that for certain shell thicknesses, i.e. between a_s=0.5 and 1 nm, the character of the ground state exciton changes from $1S_{1/2}1S_{3/2}$ to $1S_{1/2}1P_{3/2}$, see Table 1. It can be observed that the density of excitonic states increases with shell thickness: this suggests that phononic gaps are more likely to be found in core-only or core/shell structures with thin shells. However, even for a CdSe/CdTe core/shell CQD with a_s=3 nm, we have identified at least two phononic gaps, i.e., distance between subsequent excitonic states splits by more than ~30 meV. In Table 1 we have identified possible phononic gaps in the first five states of the excitonic structure – these are energy gaps between states which are greater than the energy of the longitudinal optical phonons in CdSe ($\hbar\omega_{LO} \simeq 30$ meV). It is interesting to note that only for an a_c=2 nm core-only CdSe QD, a phononic gap exists between E_{X0} and E_{X1}, while for all other structures considered (core/shell), the relaxation energy between E_{X1} and E_{X0} is not enough to trigger emission of LO phonons. In the Appendix we list all phononic gaps

Table 1
Energy difference, Δ, between the first few states in the excitonic spectra of a_c=2 nm CdSe core-only and CdSe/CdTe core/shell QDs for several different shell thicknesses, a_s; only Δ values larger than ~30 meV are listed in bold. In the bottom part of the table the characters of the first few excitons are also listed.

a_s (nm)	0	0.5	1.0	1.5	2	2.5	3
$\Delta_{E_{X0},E_{X1}}$ (meV)	**48.81**	22.69	12.86	13.99	13.60	12.27	11.49
$\Delta_{E_{X1},E_{X2}}$ (meV)	**113.77**	**55.21**	**134.89**	**138.73**	**119.57**	**97.17**	**79.57**
$\Delta_{E_{X2},E_{X3}}$ (meV)	**102.63**	**75.93**	**118.43**	**82.92**	**64.11**	**60.17**	**53.25**
$\Delta_{E_{X3},E_{X4}}$ (meV)	28.36	**85.00**	**42.37**	**44.42**	**59.89**	22.86	2.55
E_{X0}	$1S_{1/2}1S_{3/2}$	$1S_{1/2}1S_{3/2}$	$1S_{1/2}1P_{3/2}$	$1S_{1/2}1P_{3/2}$	$1S_{1/2}1P_{3/2}$	$1S_{1/2}1P_{3/2}$	$1S_{1/2}1P_{3/2}$
E_{X1}	$1S_{1/2}1P_{3/2}$	$1S_{1/2}1P_{3/2}$	$1S_{1/2}1S_{3/2}$	$1S_{1/2}1S_{3/2}$	$1S_{1/2}1S_{3/2}$	$1S_{1/2}1S_{3/2}$	$1S_{1/2}1S_{3/2}$
E_{X2}	$1S_{1/2}2S_{3/2}$	$1S_{1/2}2S_{3/2}$	$1S_{1/2}2S_{3/2}$	$1S_{1/2}2S_{3/2}$	$1S_{1/2}2S_{3/2}$	$1S_{1/2}2S_{3/2}$	$1S_{1/2}2S_{3/2}$
E_{X3}	$1S_{1/2}1P_{1/2}$	$1S_{1/2}2P_{3/2}$	$1S_{1/2}1P_{1/2}$	$1S_{1/2}1P_{1/2}$	$1S_{1/2}1P_{1/2}$	$1S_{1/2}1P_{1/2}$	$1S_{1/2}1P_{1/2}$
E_{X4}	$1S_{1/2}2P_{3/2}$	$1S_{1/2}1P_{1/2}$	$1P_{3/2}1P_{3/2}$	$1P_{3/2}1P_{3/2}$	$1S_{1/2}2P_{3/2}$	$1S_{1/2}2P_{3/2}$	$1S_{1/2}2P_{3/2}$

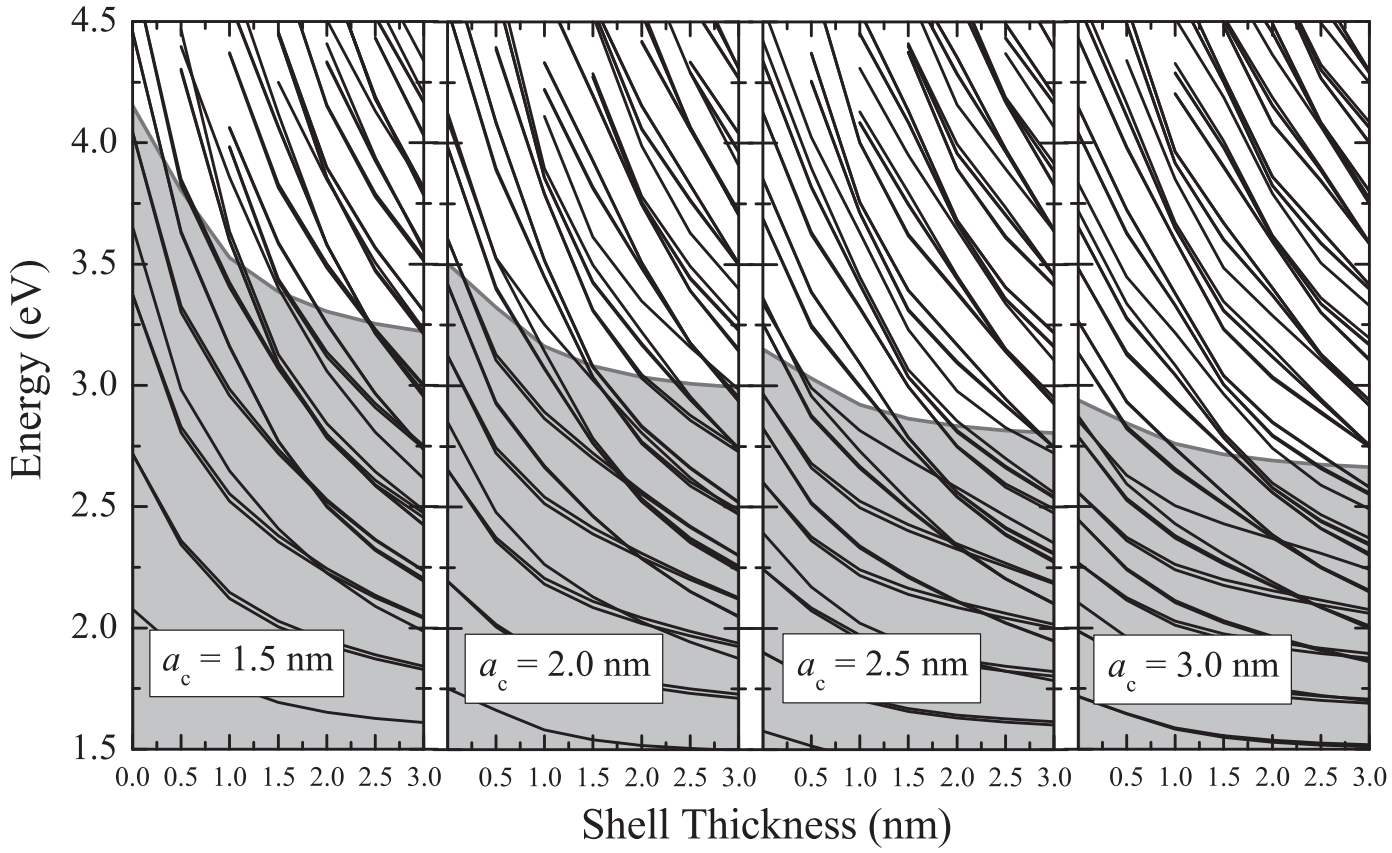

Fig. 1. CB energy levels in CdSe/CdTe type II CQDs for several core radii and varying shell thicknesses. Also shown, as a bold line, is an electron energy above the band edge equal to E_g. Below this energy (shaded), the electron has insufficient energy for MEG to occur.

in the range of energies between E_{X0} and $2E_{X0}$, for each particular CQD structure, together with excitonic characters. As shell thickness increases the number of gaps decreases, however even for a CQD with a larger shell (a_s=3 nm) we have identified at least five phononic gaps with at least two of them with the energy $> 2\hbar\omega_{LO}$.

3.2. Conduction states structure

As discussed earlier, the energy level structure of the CB and the relaxation pathways of electrons from each level will govern the cooling time and yield of highly excited electrons reaching the CBM and so will determine the efficiency of solar cells dependent on either hot carrier extraction or MEG. From the solutions of single particles Hamiltonian, Eq. (1), we extract the CB levels. These CB energy levels are shown in Fig. 1 for different core radii of 1.5, 2, 2.5, and 3 nm with shell thicknesses varying from 0 nm (core only) to 3 nm. Also shown in Fig. 1 is the threshold electron energy for MEG i.e. $1E_g$ above the lowest electron level in the CB, $1s_{1/2}$. The energy level separation is sparse for all core-only CQD considered and for thin shells, there are several gaps greater than 300 meV, i.e. phonon bottlenecks, above and below the MEG threshold. As the shell thickness increases, the levels get closer together, and changes in order occur. This reduced spacing between some levels will increase phonon cooling between them, however, there also persist gaps large compared to the phonon energy even for the CQDs with the thickest shells. Even for the most critical situation of the largest core a_c=3 nm with the thickest shell, a_s=3 nm, we have identified several phononic bottlenecks in the CB with energies of 186.59 meV, 196.77 meV, and 195.33 meV. Importantly, phonon bottlenecks remain for electrons with energy above the threshold for MEG. This means that the suppression of Auger cooling resulting from reduced wave function overlap of electrons and holes in a type II system formed by the addition of a thick shell, will not be significantly offset by a loss of phonon bottlenecks. Such a type II structure will reduce the overall electron cooling rate, not just between the lowest two energy levels as previously demonstrated [2] but, crucially for the solar cell efficiency, also for electrons with sufficient energy to cause MEG or as required in a hot carrier cell.

3.3. Comparison with experiment

Electron dynamics in CQDs can be measured using ultrafast transient absorption spectroscopy. Here pump pulses create hot excitons in a sample of CQDs, and the resulting fractional changes in the absorption of probe pulses, delayed relative to the pump pulse by a controlled amount and tuned to the first absorption peak wavelength, are measured. Filling of CB states as the electrons cool reduces the absorption of the probe in proportion to the CBM occupancy, and hence varying the pump-probe delay reveals the dynamics of electron cooling (and subsequent recombination). For this study two example CQD samples were used: a CdSe core, and the same core with a CdTe shell. The steady-state absorption spectra for these samples are shown in Fig. 2; the first absorption peak is at 2.23 eV for the CdSe CQDs, and this red-shifts to 1.74 eV when the CdTe shell is added. The spectral positions of these absorption peaks were used to estimate both the average CQD core radius and the shell thickness. For a sample of CdSe cores with an absorption peak in the same position, the mean radius of 100 CQDs has previously been measured to be $\sim 1.80 \pm 0.20$ nm using scanning transmission electron microscopy [33]. The shell thickness was estimated to be $\sim$2 nm using the calculated shift in the

absorption peak for cores of this size after the addition of a shell [34].

Using the excitonic optical dipole matrix elements and excitonic energies predicted by the CI method outlined in Section 2.1, we calculate the absorption spectra of two CQDs. We find good agreement between the lowest measured exciton peak and that found by CI calculations for an $a_c = 1.80$ nm CdSe core CQD which predict the $1S_{1/2}1S_{3/2}$ exciton to lie at 2.24 eV, Fig. 2. Such CI calculations also predict another optically active state corresponding to the $1S_{1/2}2S_{3/2}$ exciton at 2.42 eV. Unfortunately the magnitude of the dipole matrix element of the $1S_{1/2}2S_{3/2}$ transition is too small to explain the feature seen in the experimental data at this energy. However the assignment of the $1S_{1/2}2S_{3/2}$ exciton to the second peak is consistent with that made by Norris and Bawendi [35] for CdSe nanocrystals, who also noted the small oscillator strength of this exciton compared to neighbouring transitions. We show comparison of our theoretical results with experiment in Fig. 2. We modelled the absorption spectra using a sum of Gaussian peaks [36] centred on the relevant exciton energies and a cubic background [35] (to describe the continuum of transitions not included in the CI calculation). The Gaussian peak widths and cubic background were adjusted to optimize the fit to the experimental data of 12% for the size distributions of the CdSe/CdTe core/shell CQDs. A comparison of the experimental and theoretical absorption spectra shows that the $a_c = 1.80$ nm CdSe core-only CQD spectrum only agrees with experiment for the first peak, i.e. only for approximately $\sim$200 meV after the absorption edge. In order to achieve better agreement with the absorption spectrum over a wider range, we combine the theoretical absorption spectra of an $a_c = 1.80$ nm and an $a_c = 1.60$ nm CQD. The weighted average of those two spectra shows much better agreement with experiment, suggesting $\lesssim 11\%$ size dispersion in the CQD sample.

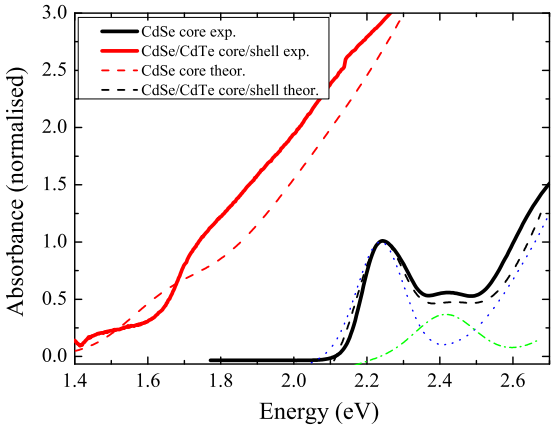

Fig. 2. Steady-state absorption spectra for a CdSe core CQD sample, and the same core with a CdTe shell (solid line) together with theoretical absorption spectra (dashed line). For CdSe core only CQD, individual absorption spectra of 1.80 nm CQD (dotted blue line) and 1.60 nm (dash-dot green line) are also depicted. (For interpretation of the references to color in this figure caption, the reader is referred to the web version of this paper.)

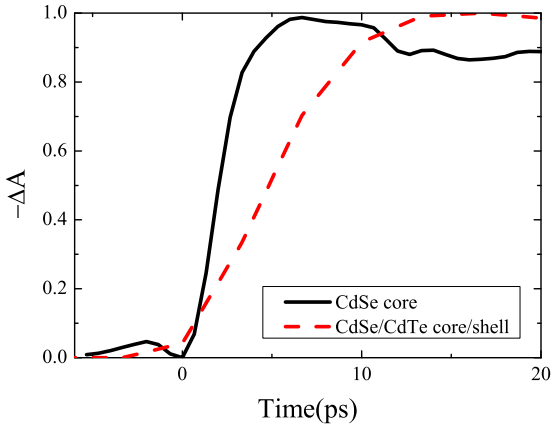

Fig. 3. Pump-induced absorption change transients data for CdSe core-only CQDs (solid line), and the same cores surrounded by 2 nm thick shell of CdTe shell (dashed line). In each case, the probe beam was tuned the first absorption peak of each CQD, and the pump beam had a photon energy of 2.76 eV and a fluence of 50 μJ/cm^2.

The rise in the pump-induced change in absorption, ΔA, for these samples is shown in Fig. 3 for a pump photon energy of 2.76 eV. The rise time for each transient provides a measure of the total relaxation rate to the CBM for each CQD, which includes contributions from both phonon and Auger cooling. The transient for the CdSe cores reaches a maximum in 5 ps, whilst for the CdSe/CdTe CQDs the peak absorption change is attained only after about 15 ps. The band edge is at a lower energy for the CdSe/CdTe CQDs and so the total energy lost during carrier relaxation is greater at 1.02 eV, compared to 0.53 eV for the CdSe CQDs; nevertheless, the rate of energy loss is still less for the CdSe/CdTe CQDs at 0.07 eV/ps, compared to 0.11 eV/ps for the CdSe CQDs. This reduced rate of energy loss for the CdSe/CdTe CQDs is consistent with the addition of the CdTe shell decreasing the rate of Auger cooling without significantly increasing the rate of phonon-mediated relaxation.

3.4. Effect on solar cell performance

The effect of shell thickness on the performance of a solar cell based on CdSe/CdTe CQDs was calculated using the results described above incorporated into a "Detailed Balance" model [24]. Detailed Balance models have been used previously to determine the dependence of solar cell efficiency on CQD band gap [17,18]. A detailed description of this approach has been given elsewhere [18] and so is only summarised here. In brief, the photogenerated current density, j_{pg}, is found by spectrally integrating the product of solar flux and a photon energy, $h\nu$, dependent quantum yield, $QY(h\nu)$. This is offset by a recombination current density, j_r, derived from black body emission of the solar cell at room temperature, and dependent on the operating voltage of the cell, V. The efficiency is then given by $\eta_{pv} = (j_{pg} - j_r)V/I$ where I is the total solar irradiance.

MEG is incorporated into the model via $QY(h\nu)$. MEG occurs above a threshold excitation energy, E_{th}, which corresponds to the minimum $h\nu$ needed to produce a hot electron in the conduction

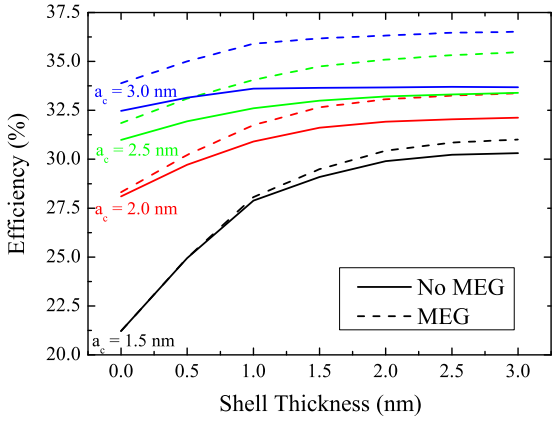

Fig. 4. Solar cell efficiency given by the Detailed Balance model for cells sensitised with CdSe/CdTe type II CQD for different core radii and for varying shell thicknesses with (dashed lines) and without the inclusion of MEG (solid lines).

band with an energy above the CBM equivalent to E_g. The energy of an absorbed photon in excess of E_g is divided between the electron and hole according to the inverse of their effective masses, m_e^* and m_h^* respectively, so that the threshold for MEG is given by [18]:

$$E_{\text{th}} = E_g\left(2+\frac{m_e^*}{m_h^*}\right) \tag{7}$$

The heavy hole and electron effective masses in CdTe are $0.8m_0$ and $0.09m_0$ respectively [37] and the electron effective mass in zinc blend CdSe is $0.11m_0$ [38]; taking the average electron effective mass for the two materials yields $E_{\text{th}} = 2.1E_g$. In the ideal case, additional excitons are created each time the excitation energy increases by a further $E_{\text{th}} - E_g$, leading to a step-like increase in quantum yield with greater $h\nu$:

$$QY(h\nu, E_g) = \sum_{n=0}^{N} \theta[h\nu, E_g + n(E_{\text{th}} - E_g)] \tag{8}$$

where θ is the Heaviside step function. Previous calculations have shown that the rate of Auger cooling in CdSe/CdTe CQDs has a strong dependence on shell thickness due to the separation of electron and hole in a type II structure [39]. In particular, the Auger cooling lifetime grows abruptly by two orders of magnitude for

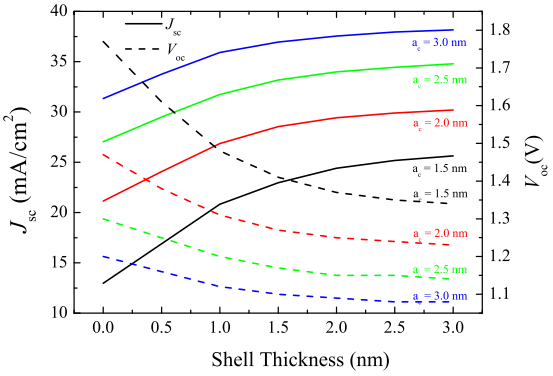

Fig. 5. Short-circuit current density, J_{sc}, and open-circuit voltage, V_{oc}, for cells sensitised with CdSe/CdTe type II CQD for different core radii and for varying shell thicknesses with the inclusion of MEG.

Table 2
List of excitonic energy differences $\Delta E_{X,i+1;X,i}$, between successive excitonic states in the energy range between E_{X0} and $2E_{X0}$ for a_c=2 nm CdSe core-only and CdSe/CdTe core/shell QDs with several different shell thicknesses, a_s; only Δ values larger than ~30 meV are listed. In the bottom part of the table the character of excitons involved in the transitions are listed too.

a_s (nm)	0	0.5	1.0	1.5	2	2.5	3
phononic gap	48.81 113.77 102.63 66.94 37.36 38.45 41.59 32.36 39.84 53.40 30.46 42.01 42.62 38.25	55.21 75.93 85.00 66.57 49.02 45.49 42.53 32.01	134.89 118.43 42.37 33.67 42.68 43.18 37.36 31.01	138.73 82.92 44.42 77.57 58.08 40.14 39.09	119.57 64.11 59.89 56.93 41.38 40.71 35.19	97.17 60.17 55.70 51.03 40.62	79.57 53.25 64.97 37.62 34.99
Initial state	$1S_{1/2}1S_{3/2}$ $1S_{1/2}1P_{3/2}$ $1S_{1/2}2S_{3/2}$ $1S_{1/2}1S_{1/2}$ $1S_{1/2}3S_{3/2}$ $1S_{1/2}3P_{3/2}$ $1P_{1/2}1P_{3/2}$ $1P_{3/2}1P_{5/2}$ $1P_{1/2}2S_{3/2}$ $1S_{1/2}5P_{3/2}$ $1P_{1/2}2P_{1/2}$ $1P_{1/2}3P_{1/2}$ $1D_{3/2}5P_{3/2}$ $1F_{7/2}4D_{7/2}$	$1S_{1/2}1P_{3/2}$ $1S_{1/2}2S_{3/2}$ $1S_{1/2}2P_{3/2}$ $1S_{1/2}3S_{3/2}$ $1S_{1/2}1S_{1/2}$ $1P_{1/2}2S_{3/2}$ $1S_{1/2}5S_{3/2}$ $2P_{1/2}3P_{1/2}$	$1S_{1/2}1S_{3/2}$ $1S_{1/2}2S_{3/2}$ $1S_{1/2}1P_{1/2}$ $1S_{1/2}1S_{1/2}$ $1S_{1/2}3S_{3/2}$ $1P_{3/2}2P_{5/2}$ $1S_{1/2}4S_{3/2}$ $2D_{3/2}1S_{3/2}$	$1S_{1/2}1S_{3/2}$ $1S_{1/2}2S_{3/2}$ $1S_{1/2}1P_{1/2}$ $1P_{3/2}1P_{5/2}$ $1S_{1/2}3S_{3/2}$ $1P_{1/2}1P_{1/2}$ $2S_{1/2}1P_{1/2}$	$1S_{1/2}1S_{3/2}$ $1S_{1/2}2S_{3/2}$ $1S_{1/2}1P_{1/2}$ $1S_{1/2}3S_{3/2}$ $1S_{1/2}3P_{3/2}$ $1P_{1/2}1P_{1/2}$ $1S_{1/2}2S_{1/2}$	$1S_{1/2}1S_{3/2}$ $1S_{1/2}2S_{3/2}$ $1S_{1/2}2P_{3/2}$ $1P_{3/2}1P_{5/2}$ $1P_{1/2}2S_{3/2}$	$1S_{1/2}1S_{3/2}$ $1S_{1/2}2S_{3/2}$ $1S_{1/2}2P_{3/2}$ $1P_{3/2}1P_{5/2}$ $1P_{1/2}2S_{3/2}$
Final state	$1S_{1/2}1P_{3/2}$ $1S_{1/2}2S_{3/2}$ $1S_{1/2}1P_{1/2}$ $1S_{1/2}3S_{3/2}$ $1S_{1/2}3P_{3/2}$ $1S_{1/2}4S_{3/2}$ $1S_{1/2}2P_{1/2}$ $1P_{3/2}1D_{5/2}$ $1S_{1/2}5P_{3/2}$ $1S_{1/2}5S_{3/2}$ $1D_{5/2}1P_{5/2}$ $1D_{5/2}3S_{3/2}$ $1F_{5/2}1D_{7/2}$ $1F_{7/2}5D_{5/2}$	$1S_{1/2}2S_{3/2}$ $1S_{1/2}2P_{3/2}$ $1S_{1/2}1P_{1/2}$ $1S_{1/2}1S_{1/2}$ $1P_{3/2}1S_{3/2}$ $1S_{1/2}2S_{1/2}$ $1S_{1/2}5P_{3/2}$ $1G_{7/2}3D_{5/2}$	$1S_{1/2}2S_{3/2}$ $1S_{1/2}1P_{1/2}$ $1P_{3/2}1P_{3/2}$ $1S_{1/2}3S_{3/2}$ $1P_{3/2}2S_{3/2}$ $1S_{1/2}4S_{3/2}$ $1S_{1/2}4P_{3/2}$ $2D_{5/2}1D_{5/2}$	$1S_{1/2}2S_{3/2}$ $1S_{1/2}1P_{1/2}$ $1P_{3/2}1P_{3/2}$ $1P_{3/2}2S_{3/2}$ $1S_{1/2}3P_{3/2}$ $1D_{5/2}1P_{3/2}$ $1P_{3/2}3D_{5/2}$	$1S_{1/2}2S_{3/2}$ $1S_{1/2}1P_{1/2}$ $1S_{1/2}2P_{3/2}$ $1P_{3/2}2S_{3/2}$ $1P_{3/2}1P_{1/2}$ $1P_{3/2}2P_{3/2}$ $2S_{1/2}1P_{1/2}$	$1S_{1/2}2S_{3/2}$ $1S_{1/2}1P_{1/2}$ $1P_{3/2}1P_{3/2}$ $1P_{3/2}2S_{3/2}$ $1P_{3/2}1P_{1/2}$	$1S_{1/2}2S_{3/2}$ $1S_{1/2}1P_{1/2}$ $1S_{1/2}3S_{3/2}$ $1S_{1/2}3P_{3/2}$ $1P_{3/2}1P_{1/2}$

shell thicknesses of 1 nm and greater. Combined with the results indicating the persistence of phonon bottlenecks with the addition of thick shells presented in this work, we thus assume that MEG is dominant for shells of 1 nm thickness or greater, exhibiting the step-like $QY(h\nu)$ described by Eq. (8), but not significant for thinner shells so that $QY(h\nu) = 1$ for $h\nu \geq E_g$ and $QY(h\nu) = 0$ for $h\nu < E_g$.

Fig. 4 shows the peak efficiency calculated using the detailed balance model for CdSe/CdTe CQDs of core radius 1.5, 2, 2.5 and 3 nm and a range of shell thicknesses, with and without MEG, where the AM1.5G solar spectrum [40] has been used. Fig. 5 shows the corresponding short-circuit current density, J_{sc}, and open-circuit voltage, V_{oc}, obtained when MEG is included in the model. The peak efficiency reaches $\approx$ 30%, 32%, 33.4% and 33.7% for structures with a_c equals 1.5, 2, 2.5 and 3 nm respectively, upon the addition of a shell largely due to the reduction in band gap. A further increase of 0.7%, 1.37%, 2.35% and 2.85% for structures with a_c equals 1.5, 2, 2.5 and 3 nm respectively, for thicker shells this is due to MEG becoming dominant over Auger cooling. This increase in efficiency with greater shell thickness is accompanied by a decrease in V_{oc}, which is more than offset by a growth in J_{sc}. Note that these V_{oc} values are obtained under idealised conditions and will tend to overestimate the values measured in real structures. It has previously been shown that the peak efficiency for a cell utilising MEG, 44%, is attained for a band gap of 0.7 eV [17]. An even greater benefit from MEG can thus be anticipated from a Type II CQD with a smaller band gap than the CdSe/CdTe system studied here.

4. Conclusions

The detailed energy level structure of CdSe/CdTe type II CQD has been calculated using a model based on $\mathbf{k} \cdot \mathbf{p}$ theory and many-particles configuration interaction method, with proper treatment of dielectric properties of such system. This has been used to investigate how the separation between levels in the CB changes as the shell thickness increases. We find that, whilst the separations between levels tend to decrease for thicker shells, there always remain steps between levels that are several times the phonon energy i.e. the so-called “phonon bottlenecks”. Moreover, such phonon bottlenecks persist at energies above the band edge both below and above the threshold for multiple exciton generation. We conclude that increasing the shell thickness in a type II CQD in order to reduce the electron-hole wave-function overlap, and thus the rate of Auger cooling, will not also significantly increase the rate of phonon relaxation, and the total electron cooling rate will therefore be reduced. Transient absorption measurements on a sample of CdSe CQDs with and without a 2 nm thick CdTe shell confirm that the overall electron cooling time is increased for the CdSe/CdTe structure. Further, using a detailed balance model, we have calculated that this reduced cooling rate, and the consequent increase in MEG quantum yield, results in an increase of the ideal efficiency of solar cells utilising CdSe/CdTe CQDs to 36.5% for thick shells.

Acknowledgements

The authors acknowledge the EPSRC UK Grant “Enhanced multiple exciton generation in colloidal quantum dots” (EP/K008587/1) for financial support. We also acknowledge the EU-COST project “MultiscaleSolar” (MP1406) and the Royal Society (No.: RG120558) Grant “High Performance Computing in Modelling of Innovative Photo-Voltaic Devices”. We acknowledge help from the N8 Research Partnership and Science and Technology Facilities Council for providing the computational resources used to conduct this research. We would also like to express our gratitude to W. Flavell for useful discussions.

Appendix

See Table 2.

References

[1] M. Beard, R. Ellingson, Multiple exciton generation in semiconductor nanocrystals: toward efficient solar energy conversion, Laser Photonics Rev. 2 (5) (2008) 377–399.
[2] A. Pandey, P. Guyot-Sionnest, Slow electron cooling in colloidal quantum dots, Science 322 (5903) (2008) 929–932.
[3] A.J. Nozik, Spectroscopy and hot electron relaxation dynamics in semiconductor quantum wells and quantum dots, Annu. Rev. Phys. Chem. 52 (1) (2001) 193–231 11326064.
[4] C. Smith, D. Binks, Multiple exciton generation in colloidal nanocrystals, Nanomaterials 4 (1) (2013) 19.
[5] P.V. Kamat, Quantum dot solar cells. the next big thing in photovoltaics, J. Phys. Chem. Lett. 4 (6) (2013) 908–918.
[6] C.A. Nelson, N.R. Monahan, X.-Y. Zhu, Exceeding the Shockley–Queisser limit in solar energy conversion, Energy Environ. Sci. 6 (2013) 3508–3519.
[7] A. Al-Otaify, S.V. Kershaw, S. Gupta, A.L. Rogach, G. Allan, C. Delerue, D.J. Binks, Multiple exciton generation and ultrafast exciton dynamics in HgTe colloidal quantum dots, Phys. Chem. Chem. Phys. 15 (2013) 16864–16873.
[8] M. Cadirci, S.K. Stubbs, S.J.O. Hardman, O. Masala, G. Allan, C. Delerue, N. Pickett, D.J. Binks, Ultrafast exciton dynamics in InAs/ZnSe nanocrystal quantum dots, Phys. Chem. Chem. Phys. 14 (2012) 15166–15172.
[9] M. Cadirci, S.K. Stubbs, S.M. Fairclough, E.J. Tyrrell, A.A.R. Watt, J.M. Smith, D. J. Binks, Ultrafast exciton dynamics in type II ZnTe-ZnSe colloidal quantum dots, Phys. Chem. Chem. Phys. 14 (2012) 13638–13645.
[10] S.J.O. Hardman, D.M. Graham, S.K. Stubbs, B.F. Spencer, E.A. Seddon, H.-T. Fung, S. Gardonio, F. Sirotti, M.G. Silly, J. Akhtar, P. O'Brien, D.J. Binks, W.R. Flavell, Electronic and surface properties of PbS nanoparticles exhibiting efficient multiple exciton generation, Phys. Chem. Chem. Phys. 13 (2011) 20275–20283.
[11] C.T. Smith, M.A. Leontiadou, R. Page, P. O'Brien, D.J. Binks, Ultrafast charge dynamics in trap-free and surface-trapping colloidal quantum dots, Adv. Sci., 2, 2015, http://dx.doi.org/10.1002/advs.201500088.
[12] T. Inoshita, H. Sakaki, Electron relaxation in a quantum dot: significance of multiphonon processes, Phys. Rev. B 46 (1992) 7260–7263.
[13] U. Bockelmann, G. Bastard, Phonon scattering and energy relaxation in two-, one-, and zero-dimensional electron gases, Phys. Rev. B 42 (1990) 8947–8951.
[14] S. Tomić, Intermediate-band solar cells: influence of band formation on dynamical processes in InAs/GaAs quantum dot arrays, Phys. Rev. B 82 (2010) 195321.
[15] P. Kambhampati, Hot exciton relaxation dynamics in semiconductor quantum dots: radiationless transitions on the nanoscale, J. Phys. Chem. C 115 (45) (2011) 22089–22109.
[16] P. Guyot-Sionnest, B. Wehrenberg, D. Yu, Intraband relaxation in CdSe nanocrystals and the strong influence of the surface ligands, J. Chem. Phys. 123 (7) (2005) –.
[17] M.C. Hanna, A.J. Nozik, Solar conversion efficiency of photovoltaic and photoelectrolysis cells with carrier multiplication absorbers, J. Appl. Phys. 100 (7) (2006) 074510.
[18] D.J. Binks, Multiple exciton generation in nanocrystal quantum dots—controversy, current status and future prospects, Phys. Chem. Chem. Phys. 13 (2011) 12693–12704.
[19] M.C. Beard, J.M. Luther, O.E. Semonin, A.J. Nozik, Third generation photovoltaics based on multiple exciton generation in quantum confined semiconductors, Acc. Chem. Res. 46 (6) (2013) 1252–1260 23113604.
[20] U. Aeberhard, R. Vaxenburg, E. Lifshitz, S. Tomić, Fluorescence of colloidal PbSe/PbS QDs in NIR luminescent solar concentrators, Phys. Chem. Chem. Phys. 14 (2012) 16223–16228.
[21] E.J. Tyrrell, S. Tomić, Effect of correlation and dielectric confinement on $1s^{(e)}_{1/2}$ $ns^{(h)}_{3/2}$ excitons in CdTe/CdSe and CdSe/CdTe type-II quantum dots, J. Phys. Chem. C 119 (22) (2015) 12720–12730.
[22] M.D. Peterson, L.C. Cass, R.D. Harris, K. Edme, K. Sung, E.A. Weiss, The role of ligands in determining the exciton relaxation dynamics in semiconductor quantum dots, Annu. Rev. Phys. Chem. 65 (1) (2014) 317–339 24364916.
[23] G.H. Carey, A.L. Abdelhady, Z. Ning, S.M. Thon, O.M. Bakr, E.H. Sargent, Colloidal quantum dot solar cells, Chem. Rev. 115 (23) (2015) 12732–12763.
[24] W. Shockley, H.J. Queisser, Detailed balance limit of efficiency of p-n junction solar cells, J. Appl. Phys. 32 (3) (1961) 510–519.
[25] E.P. Pokatilov, V.A. Fonoberov, V.M. Fomin, J.T. Devreese, Development of an eight-band theory for quantum dot heterostructures, Phys. Rev. B 64 (2001) 245328.

[26] A.L. Efros, M. Rosen, Quantum size level structure of narrow-gap semiconductor nanocrystals: effect of band coupling, Phys. Rev. B 58 (1998) 7120–7135.
[27] N. Vukmirović, S. Tomić, Plane wave methodology for single quantum dot electronic structure calculations, J. Appl. Phys. 103 (10) (2008) 103718.
[28] E.J. Tyrrell, J.M. Smith, Effective mass modeling of excitons in type-II quantum dot heterostructures, Phys. Rev. B 84 (2011) 165328.
[29] P.G. Bolcatto, C.R. Proetto, Partially confined excitons in semiconductor nanocrystals with a finite size dielectric interface, J. Phys.: Condens. Matter 13 (2) (2001) 319.
[30] E. Menéndez-Proupin, C. Trallero-Giner, Electric-field and exciton structure in CdSe nanocrystals, Phys. Rev. B 69 (12) (2004) 125336.
[31] M.B. Mohamed, D. Tonti, A. Al-Salman, A. Chemseddine, M. Chergui, Synthesis of high quality zinc blende CdSe nanocrystals, J. Phys. Chem. B 109 (21) (2005) 10533–10537.
[32] N. McElroy, R. Page, D. Espinbarro-Valazquez, E. Lewis, S. Haigh, P. O'Brien, D. Binks, Comparison of solar cells sensitised by CdTe/CdSe and CdSe/CdTe core/shell colloidal quantum dots with and without a cds outer layer, Thin Solid Films 560 (0) (2014) 65–70, european Materials Research Society (E-MRS) Spring Meeting 2013 Symposium B: Organic and hybrid interfaces in excitonic solar cells: from fundamental science to applications.
[33] E.A. Lewis, R.C. Page, D.J. Binks, T.J. Pennycook, P. O'Brien, S.J. Haigh, Probing the core-shell-shell structure of CdSe/CdTe/CdS type II quantum dots for solar cell applications, J. Phys.: Conf. Ser. 522 (1) (2014) 012069.
[34] M.A. Leontiadou, E.J. Tyrrell, C.T. Smith, D. Espinbarro-Velasquez, J. Miloszewski, T. Walsh, D. Binks, S. Tomić, Influence of elevated radiative lifetime on efficiency of CdSe/CdTe type II colloidal quantum dot based solar cells, Sol. Energy Mater. Sol. Cells, submitted for publication.
[35] D.J. Norris, M.G. Bawendi, Measurement and assignment of the size-dependent optical spectrum in CdSe quantum dots, Phys. Rev. B 53 (1996) 16338–16346.
[36] V.I. Klimov, Optical nonlinearities and ultrafast carrier dynamics in semiconductor nanocrystals, J. Phys. Chem. B 104 (26) (2000) 6112–6123.
[37] Landolt-Bornstein, III/23a, 95–98, 1989.
[38] I.C. Hernandez, Optical properties and electronic structure in II-VI semiconductors materials and their applications, New York, 2001.
[39] S.Tomić, J.M. Miloszewski, E.J. Tyrrell, D.J. Binks, Design of core/shell colloidal quantum dots for MEG solar cells, IEEE J. Photovolt. 6 (2016) 179–184.
[40] ⟨http://rredc.nrel.gov/solar/spectra/am1.5/⟩.